

Published in final edited form as:

*Neuroimage*. 2010 September ; 52(3): 884–896. doi:10.1016/j.neuroimage.2009.11.060.

## Effect of Hemodynamic Variability on Granger Causality Analysis of fMRI

Gopikrishna Deshpande<sup>1</sup>, K. Sathian<sup>2,3</sup>, and Xiaoping Hu<sup>1</sup>

<sup>1</sup> Coulter Department of Biomedical Engineering, Georgia Institute of Technology and Emory University, Atlanta, GA, USA

<sup>2</sup> Departments of Neurology, Rehabilitation Medicine and Psychology, Emory University, Atlanta, GA, USA

<sup>3</sup> Rehabilitation R&D Center of Excellence, Atlanta VAMC, Decatur, GA, USA

### Abstract

In this work, we investigated the effect of the regional variability of the hemodynamic response on the sensitivity of Granger causality (GC) analysis of functional magnetic resonance imaging (fMRI) data to neuronal causal influences. We simulated fMRI data by convolving a standard canonical hemodynamic response function (HRF) with local field potentials (LFPs) acquired from the macaque cortex and manipulated the causal influence and neuronal delays between the LFPs, the hemodynamic delays between the HRFs, the signal to noise ratio (SNR) and the sampling period (TR) in order to assess the effect of each of these factors on the detectability of the neuronal delays from GC analysis of fMRI. In our first bivariate implementation, we assumed the worst case scenario of the hemodynamic delay being at the empirical upper limit of its normal physiological range and opposing the direction of neuronal delay. We found that, in the absence of HRF confounds, even tens of milliseconds of neuronal delays can be inferred from fMRI. However, in the presence of HRF delays which opposed neuronal delays, the minimum detectable neuronal delay was hundreds of milliseconds. In our second multivariate simulation, we mimicked the real situation more closely by using a multivariate network of four time series and assumed the hemodynamic and neuronal delays to be unknown and drawn from a uniform random distribution. The resulting accuracy of detecting the correct multivariate network from fMRI was well above chance and was up to 90% with faster sampling. Generically, under all conditions, faster sampling and low measurement noise improved the sensitivity of GC analysis of fMRI data to neuronal causality.

### Index Terms

Functional MRI; Granger Causality; Hemodynamic Variability; Minimum Detectable Neuronal Delay

---

© 2009 Elsevier Inc. All rights reserved.

Corresponding Author: Xiaoping Hu, Ph.D., Wallace H. Coulter Department of Biomedical Engineering, Georgia Institute of Technology and Emory University, 101 Woodruff Circle, Suite 2001, Atlanta, GA 30322, USA, Phone- 404 712 2615, Fax- 404 712 2707, xhu@bme.gatech.edu.

**Publisher's Disclaimer:** This is a PDF file of an unedited manuscript that has been accepted for publication. As a service to our customers we are providing this early version of the manuscript. The manuscript will undergo copyediting, typesetting, and review of the resulting proof before it is published in its final citable form. Please note that during the production process errors may be discovered which could affect the content, and all legal disclaimers that apply to the journal pertain.

## INTRODUCTION

Investigation of effective connectivity in brain networks, i.e. the causal influence one neuronal system exerts over another (Friston, 1995), is being increasingly recognized as an important tool for understanding brain function in neuroimaging studies employing functional magnetic resonance imaging (fMRI). One approach to investigation of effective brain connectivity that has gained prominence of late is Granger causality (GC) analysis. It is based on the principle of temporal precedence, wherein, if the knowledge of the past temporal evolution of the signal from a region of interest (ROI) *A* increases the predictability of the future temporal evolution of the signal in another ROI *B*, then *A* is said to Granger-cause *B* (Granger, 1969). This approach has been mathematically formalized using vector autoregressive (VAR) models, initially using electroencephalographic (EEG) data (Kus, Kaminski, & Blinowska, 2004; Blinowska, Kus, & Kaminski, 2004; Kaminski, Ding, Truccolo, & Bressler, 2001). Later, this approach was successfully applied to fMRI data for investigating brain networks underlying sensory (Stilla, Deshpande, Laconte, Hu, & Sathian, 2007; Deshpande, Hu, Stilla, & Sathian, 2008; Stilla, Hanna, Mariola, Deshpande, Hu, & Sathian, 2008), motor (Deshpande, LaConte, James, Peltier, & Hu, 2009; Abler, et al., 2006) and cognitive tasks (Roebroek, Formisano, & Goebel, 2005). Various implementations of GC have been reported which include bivariate (Roebroek, Formisano, & Goebel, 2005), multivariate (Deshpande, Hu, Stilla, & Sathian, 2008), time-domain (Abler, et al., 2006) and frequency-domain (Deshpande, LaConte, James, Peltier, & Hu, 2009) analyses. GC offers certain distinct advantages over other approaches for investigating effective connectivity such as structural equation models (SEM) (Zhuang, LaConte, Peltier, Zhang, & Hu, 2005) and dynamic causal models (DCM) (Friston, Harrison, & Penny, 2003). First, unlike SEM and DCM, GC only requires the pre-specification of the regions of interest (ROIs) and does not make any assumptions about the connections between them. Second, it has the potential to work with a large number of ROIs, the constraint being that the number of temporal acquisitions must be greater than the number of ROIs: this constraint is easily satisfied in typical fMRI experiments. Third, it is based on temporal precedence, which is intuitively linked to the concept that brain function typically requires a causal chain of events involving multiple regions. Finally, being a stochastic model, it allows for the complexities involved in brain interactions which can sometimes be oversimplified by deterministic models such as DCM.

Notwithstanding the advantages that GC offers over other approaches, there are certain fundamental unanswered questions about the applicability of GC to fMRI. First, fMRI measures signals that result from smoothing of the neuronal activity by the hemodynamic response function (HRF) and down-sampling due to the speed of MR acquisition; these signals are not direct measures of neural activity. It has been shown that the shape and magnitude of the HRF varies across brain regions and individuals (Aguirre, Zarahn, & D'Esposito, 1998; Silva & Koretsky, 2002; Handwerker, Ollinger, & D'Esposito, 2004). Only a part of this variance is attributable to neuronal activity and various other factors such as vasculature differences, baseline cerebral blood flow, hematocrit, alcohol/caffeine/lipid ingestion, partial volume imaging of veins, global magnetic susceptibilities, slice timing differences and pulse or respiration differences (Buxton, 2002; Levin, et al., 1998; Levin, et al., 2001; Noseworthy, Alfonsi, & Bells, 2003; Handwerker, Ollinger, & D'Esposito, 2004) are responsible for the variability of the HRF. Therefore, HRF variability has the potential to confound the inference of neuronal causality from fMRI data. As a remedy to this, previous studies have suggested that the modulation of Granger causality between the fMRI time series as a function of the experimental context be investigated (Roebroek, Formisano, & Goebel, 2005). According to this reasoning, such modulation would rule out HRF variability as the sole factor determining the results since, generally speaking, neuronal activity, and not the various other factors contributing to HRF variability listed above, is modulated by

the experimental context (exceptions to the above rule, such as experiments involving anesthesia, exist). This approach is useful, but limits the applicability of GC to tasks which involve modulating an experimental context and excludes tasks which employ a single experimental context and resting state. It also limits the interpretation of the causal connections obtained from GC analysis to those paths which change with experimental context.

In this work, we performed simulations in order to quantitatively characterize the effect of HRF variability on fMRI-based GC analysis in terms of physiological parameters such as neuronal and hemodynamic delays and experimental parameters such as repetition time (TR) of the MR data acquisition and the signal to noise ratio (SNR) of the fMRI data. In doing so, we also investigated the minimum detectable neuronal delay using GC analysis of fMRI in the face of variation in the above factors of interest. The general framework for the simulations was as follows: The ground truth for the causal relationships between interacting brain regions was provided by electrophysiological signals, specifically local field potentials (LFPs) acquired from the relevant ROIs in the brain, because they have the temporal resolution to capture the scale at which causal neuronal relationships occur and are a direct measure of neuronal activity. Subsequently, the neuronal data were smoothed by the HRF and down-sampled to produce simulated fMRI data. This strategy is in agreement with our understanding of the physiological basis of the fMRI signal (Logothetis, Pauls, Augath, Trinath, & Oeltermann, 2001). By manipulating the properties of the HRF, the amount of neuronal delay, TR and the presence or absence of measurement noise, the corresponding effects on inferences obtained from fMRI-based GC analysis were evaluated.

## METHODS

We illustrate the effect of HRF confounds on fMRI-based GC analysis, using both bivariate and multivariate models, within the framework described in the previous section. In order to make the simulations realistic, we utilized three channels of LFP signals recorded at a sampling frequency of 1 KHz from the macaque lateral intraparietal area during a reach and saccade task (the data are freely available in the Chronux database: [www.chronux.org](http://www.chronux.org)). This is a significant difference from previous approaches (e.g., Roebroek, Formisano, & Goebel, 2005), which have assumed the realizations of autoregressive processes to represent the LFP signals. The mathematical synthesis of simulated signals provides the advantage of choosing model parameters in order to manipulate the causal relationship between the time series. However, the model parameters also impose a uniform structure on the simulated signals, which is rarely observed in real world signals. For example, the diagonal elements of the autoregressive model impose a uniform spectral power in the simulated signals which can influence the statistical significance of Granger causality obtained from surrogate data (Pandit & Wu, 1983) in a favorable way and hence overestimate the performance of GC analysis in relationship to that obtained from real data. In this work, we circumvented the disadvantage using two strategies. In the first approach, a single channel of real LFP data,  $x(n)$ , was chosen and a simple delay was introduced to obtain the other time series,  $y(n)$ . Accordingly,

$$y(n) = x(n - d_n) \quad (1)$$

where  $d_n$  is the neuronal delay. Supposing we assume that  $x(n)$  and  $y(n)$  correspond to LFPs from neuronal populations  $X$  and  $Y$ , respectively, this approach assumes that the neuronal activity at  $X$  simply replicates at  $Y$  after a temporal delay of  $d_n$  ms and that the contribution of intrinsic dynamics at  $Y$  is zero. In the second approach, we relaxed the above condition

and assumed that the activity at  $Y$  is a weighted sum of its own intrinsic dynamics which is unrelated to  $X$  plus the delayed influence from  $X$ . Accordingly,

$$y(n) = [C \times x(n - d_n)] + [(1 - C) \times y_{intrinsic}(n)] \quad (2)$$

In this formulation,  $x(n)$  was obtained from a single channel of the real LFP data and  $y_{intrinsic}(n)$  was obtained by randomizing the phase of a different channel of real LFP data. Thus, the intrinsic dynamics of  $Y$  not only had a magnitude spectrum different from that of  $X$ , it was also not causally related to  $X$ . Therefore, the causal relationship between  $X$  and  $Y$  was determined by both the neuronal delay,  $d_n$ , and the factor  $C$ , which controlled the strength of the causal influence exerted by  $X$  on  $Y$ . We varied  $C$  from 0.5 to 0.9 in steps of 0.2. When  $C=0.5$ , the contribution from the causal influence and intrinsic dynamics was equal and hence represents a weak causal influence because 50% of the phase in  $y(n)$  was drawn from a random process. On the other hand,  $C=0.9$  represents a strong causal influence from  $X$  to  $Y$ .  $C=1$  represents the case of a simple neuronal delay shown in Eq.1. This simulation framework provided the capability to manipulate the causal relationship between the time series in addition to investigating the variability of HRF. Also, the inherent causal relationships between the recorded LFP time series was not a factor in our simulations since the causal relationships were artificially induced independently for each channel of the recorded data. Using real LFP data, however, overcame the disadvantage of the uniform structure of the signal obtained from synthetic data, thus enabling our simulations to better mimic the real world scenario.

### The Bivariate Case

In the bivariate implementation, we obtained  $x(n)$  and  $y(n)$  using both the simple delay and simple delay plus intrinsic dynamics approaches described above such that  $x(n)$  had a causal influence on  $y(n)$ . The neuronal delay,  $d_n$ , was varied from 1 ms to 1000 ms in steps of 5 ms.  $x(n)$  and  $y(n)$  were convolved with canonical HRFs,  $h_1(n)$  and  $h_2(n)$  respectively, obtained from two gamma functions with standard parameters as used as in SPM2 (Friston, Holmes, & Ashburner, 1999), such that  $h_1(n)$  lagged  $h_2(n)$  by a hemodynamic delay of  $d_h$  which assumed values of 0.5 s and 2.5 s. The choice of the range of the hemodynamic delay is in agreement with previous studies (Handwerker, Ollinger, & D'Esposito, 2004) which have shown that the normal range of physiological variability, calculated by using the offset between the canonical HRF and the measured HRF from different regions, has an empirical upper limit of 2.5 s with a mean around 0.5 s. Though HRF variability across both subjects and brain regions is around 4 s, inter-regional variability within the same subject, which is more relevant to Granger causality analysis, is in agreement with our assumptions. Each of the gamma functions used in the HRFs is a function of the scale parameter  $\theta$  and shape parameter  $k$ . The shape parameter of the first gamma function is a ratio of the delay of the response to its dispersion and determines the shape of the HRF peak. The hemodynamic variability across brain regions is mainly characterized by the variability of a combination of factors, primarily, the time to peak and onset time (Handwerker, Ollinger, & D'Esposito, 2004). Thus, by varying the shape parameter for the first gamma function, we were able to introduce a hemodynamic delay  $d_h$  between the HRFs which simultaneously changed the time to peak and onset time of  $h_2(n)$  such that it was ahead of those of  $h_1(n)$ . Consequently, the hemodynamic delay opposed the direction of neuronal delay, which represents the worst-case scenario in which the hemodynamic confounds could affect fMRI-based GC analysis. The opposite case, wherein the hemodynamic delay aids the neuronal delay, is also plausible since it has been shown that the measured HRF can lead or lag the canonical HRF with the lead limit being 2.5 s and the lag limit being 1.5 s. However, we only consider the case where in the hemodynamic delay opposes the neuronal delay since it has the most

confounding effect on the inference of GC from fMRI. Though the *magnitude* of GC inferred from fMRI could be contaminated if the HRF delay aids the neuronal delay, the *direction* of the causal influence is accurately determined in this case in contrast to the case when the HRF delay opposes the neuronal delay. Hence, we consider the latter case here. The signals resulting from the convolution of the LFP time series with the HRFs were down-sampled to obtain simulated fMRI time series  $x'(n)$  and  $y'(n)$  at TRs of 0.5, 1, 1.5 and 2 seconds, respectively. Let  $C_d$  represent the dominant Granger causal influence from  $x'(n)$  to  $y'(n)$  obtained by subtracting the influence from  $y'(n)$  to  $x'(n)$  from that of  $x'(n)$  to  $y'(n)$ . The individual causal strengths between  $x'(n)$  and  $y'(n)$  were obtained using the vector autoregressive model as in Deshpande et al (Deshpande, Hu, Stilla, & Sathian, 2008). Due to smoothing by the HRF, both  $x'(n) \rightarrow y'(n)$  and  $y'(n) \rightarrow x'(n)$  may be significant when the neuronal influence is from  $x'(n)$  to  $y'(n)$ , in which case  $x'(n) \rightarrow y'(n)$  is likely to be higher than  $y'(n) \rightarrow x'(n)$  (Roebroeck, Formisano, & Goebel, 2005). Calculating the dominant directional influence tests whether this is indeed the case. Subsequently, both  $x(n)$  and  $y(n)$  were convolved with identical canonical HRFs  $h_I(n)$  and the resulting time series were down-sampled to obtain simulated fMRI signals  $x''(n)$  and  $y''(n)$ . Let  $C_o$  represent the dominant Granger causal influence from  $x''(n)$  to  $y''(n)$ . Subsequently, we ascertained the mean ( $\mu$ ) and standard deviation ( $\delta$ ) of the empirical null distributions obtained from the GC analysis of surrogate data derived by randomizing the phase of the simulated fMRI data (Theiler, Eubank, Longtin, Galdrikian, & Farmer, 1992; Deshpande, Hu, Stilla, & Sathian, 2008). We defined parameters  $\rho_o$  and  $\rho_d$  as given below in order to characterize the detectability of the neuronal delay in the absence and presence of hemodynamic confounds, respectively.

$$\rho_o(d_n) = \frac{C_o(d_n) - \mu_o(d_n)}{\sigma_o(d_n)} \quad (3)$$

$$\rho_d(d_n) = \frac{C_d(d_n) - \mu_d(d_n)}{\sigma_d(d_n)} \quad (4)$$

$\rho_o$  (or  $\rho_d$ ) characterizes the distance between  $C_o$  (or  $C_d$ ) and the mean of the empirical null distribution in terms of its standard deviation. As long as  $\rho_o$  (or  $\rho_d$ ) is greater than 3, i.e. the GC obtained from simulated fMRI is three standard deviations away from the mean of the null distribution, we can be confident that the corresponding causal influence will be recognized as a significant one. The greater the value of  $\rho_o$  (or  $\rho_d$ ), the greater is the robustness and reliability of the causal influence derived from fMRI. If  $\rho_o$  (or  $\rho_d$ ) were to be less than 3 for any  $d_n$  (or  $d_h$ ) and greater than 3 for the following neuronal delays, the corresponding neuronal delay  $d^{min}$ , defined as the point of inflection, would represent the minimum detectable delay using fMRI-based GC.  $\rho_o$  and  $\rho_d$  were obtained from all the channels and trials of the LFP data available in the Chronux database using both the simple delay and simple delay plus intrinsic dynamics approaches described above. The above procedure was repeated with the addition of measurement noise such that the resulting simulated fMRI time series had an SNR of 1. In order to determine the SNR, defined as the ratio of the signal power to the noise power, the signal power was first calculated by obtaining the sum of the amplitude squares of each simulated time series normalized by its length. Subsequently, the noise time series was generated using MATLAB's inbuilt random number generator such that it matched the power of the simulated time series data. The signal and noise time series were then added to obtain the noise corrupted simulated data with SNR equal to one.

## The Multivariate Case

In the multivariate implementation of the simulations using simple delay, we sliced each LFP time series  $x(n)$  into three parts,  $x_1(n)$ ,  $x_2(n)$  and  $x_3(n)$  with lengths  $l_1$ ,  $l_2$  and  $l_3$  ms, respectively, and as shown in Fig. 1 such that  $x_1(n)$  began  $d_2$  ms after the end of  $x_3(n)$  and  $x_2(n)$  began  $d_1$  ms after the beginning of  $x_3(n)$ . Accordingly,  $x_1(n)$  leads  $x_2(n)$  by  $l_3 - d_1 + d_2$  ms and  $x_2(n)$  leads  $x_3(n)$  by  $d_1$  ms. Time series  $x_4(n)$  was defined to begin at  $l_3$  ms and end at  $l_2 + d_1$  ms. Consequently,  $x_4(n)$  leads  $x_2(n)$  by  $l_3 - d_1$  ms and  $x_1(n)$  leads  $x_4(n)$  by  $d_2$  ms. Due to the above-mentioned delays between the time series, we should obtain the network in Fig. 2 as the ground truth from the neuronal data. This scheme was designed to incorporate a mediated influence from  $x_1(n)$  to  $x_3(n)$  via  $x_2(n)$  which should not be inferred as a direct connection from  $x_1(n)$  to  $x_3(n)$  in fMRI data since  $x_1(n)$  and  $x_3(n)$  did not have an overlap. Also, in addition to a direct connection from  $x_1(n)$  to  $x_2(n)$ , a mediated path via  $x_4(n)$  must be inferred since  $x_1(n)$  leads  $x_4(n)$ , which in turn leads  $x_2(n)$ . Since these types of situations are commonly observed in brain networks, we felt that it was important to model them in our multivariate simulations.

In the multivariate implementation of the simulations using simple delay plus intrinsic dynamics approach,  $x_1(n)$ ,  $x_2(n)$ ,  $x_3(n)$  and  $x_4(n)$  were first obtained from a single LFP channel as was done in the simple delay approach. Subsequently,  $y_1(n)$ ,  $y_2(n)$ ,  $y_3(n)$  and  $y_4(n)$  were defined as follows

$$y_1(n) = x_1(n) \quad \text{and} \quad y_j(n) = \left[ C \times x_j(n) \right] + \left[ (1 - C) \times y_j^{\text{intrinsic}}(n) \right] \quad \text{for} \quad j=2, 3, 4 \quad (5)$$

Where  $y_j^{\text{intrinsic}}$  was obtained by randomizing the phase of a separate LFP channel for each  $j$  which was different from the one used to obtain  $x_1(n)$ .

The delays between the time series were picked from a uniform random distribution with lower and upper limits of 1 ms and 500 ms, respectively, subject to the constraint that it should preserve the basic structure of the network given in Fig. 2. Similar to the bivariate case,  $x_1(n)/y_1(n)$ ,  $x_2(n)/y_2(n)$ ,  $x_3(n)/y_3(n)$  and  $x_4(n)/y_4(n)$  were smoothed by HRFs  $h_1(n)$ ,  $h_2(n)$ ,  $h_3(n)$  and  $h_4(n)$ , respectively, with the shape parameter of each of the HRFs chosen such that the time to peak and onset time assumed random values varying from 0 to 2.5 ms. The resultant time series were down-sampled to achieve TRs of 0.5, 1, 1.5 and 2 s, respectively. As before, the choice of the limits of the hemodynamic variability was dictated by its normal physiological range (Handwerker, Ollinger, & D'Esposito, 2004). For simulations with simple delay plus intrinsic dynamics, two cases were considered. In the first case, the parameter  $C$  was assigned deterministic values of 0.5, 0.7 and 0.9 as in the bivariate case. In the second case,  $C$  assumed a random value between 0.5 and 1. Randomization of the neuronal delay, proportion of intrinsic dynamics and hemodynamic variability mimics real situations where in the precise values for these parameters are typically not available during neuroimaging experiments and it is difficult to dissociate the neuronal and hemodynamic factors contributing to HRF variability. Measurement noise was added to the fMRI time series such that the resulting fMRI time series had an SNR of 1. The procedure described above was repeated 10,000 times in order to adequately sample the random distributions used for the neuronal and hemodynamic delays. The number of times the correct multivariate network was ascertained from fMRI was determined and the corresponding percentage accuracy was calculated. The above procedure was repeated by considering each channel of LFP data  $x(n)$ .

## RESULTS AND DISCUSSION

### The Bivariate Case

**Without HRF Confound**—The detectability of the neuronal delay,  $d_n$ , from GC derived from fMRI as characterized by  $\rho_o$  is shown in Fig. 3 (simple delay) and Fig. 4 (simple delay plus intrinsic dynamics) as a function TR and noise. The corresponding points of inflection are shown in Table.1. The error bars indicate the standard deviation of  $\rho_o$  obtained across different LFP channels. It can be seen that, in the absence of opposing hemodynamic delays,  $\rho_o$  was well above the threshold for all TRs even in the presence of noise for a simple delay. This indicates that GC derived from fMRI was sensitive to even tens of millisecond delays in the corresponding neuronal data. However, the sensitivity decreased with longer TRs, shorter neuronal delays and the presence of measurement noise. Noise and slower TR also stunted the rate of increase of  $\rho_o$  with increasing neuronal delay. Similar inferences can be drawn for the case of simple delay plus intrinsic dynamics shown in Fig. 4, though unlike Fig. 3,  $\rho_o$  was below the threshold of 3 for tens milliseconds of neuronal delays (Table.1). In addition, it can be inferred from Fig. 4 that weaker causal influences with higher proportion of intrinsic neuronal dynamics (i.e. lower values of  $C$  in Eq.2) decreased the sensitivity of GC. It is noteworthy that  $\rho_o$  peaked in the absence of noise (and abruptly jumped in the presence of noise) around 500 ms for a TR of 0.5 s (Figs. 3 and 4), indicating that when the neuronal delay and the sampling period were exactly matched, there was a type of resonance effect where in the sensitivity of GC derived from fMRI was high. This is agreement with the theoretical analysis of Wei (Wei, 1982) showing that matching the scale of causal influence and sampling increases the sensitivity of GC.

In the literature, skepticism exists about the ability of GC derived from fMRI to detect neuronal delays which are typically an order of magnitude lesser than the TR of fMRI acquisition. However, our results seems to indicate that though the sensitivity of fMRI-based GC measures diminishes with decreasing neuronal delay, in the absence of HRF confounds, it could indeed be used to infer neuronal causality reliably. Below, we provide an intuitive argument as to why this might be the case.

Given an LFP time series  $x(n)$  and HRF  $h_I(n)$ , the corresponding unsampled fMRI time series is given by  $x''(n) = x(n) * h_I(n)$ , where “\*” represents the convolution operation. Consequently, if  $x(n)$  were to be shifted by  $d$  ms, then we have  $x(n-d) * h_I(n) = x''(n-d)$ . Since convolution is a form of temporal aggregation, it has the potential to make the unidirectional causal influence from  $x(n-d)$  to  $x(n)$  to appear as a bidirectional influence between  $x''(n)$  and  $x''(n-d)$ . This has been theoretically illustrated by Wei (Wei, 1982) wherein it is shown that temporal aggregation increases the instantaneous correlation between the time series which in turn “leaks” into the causal domain making causality appear bidirectional. As a proof of principle, the instantaneous correlation is less and the inferred causality is unidirectional, if one of the two time series were to be a white noise process (Wei, 1982). However, as noted before, the influence  $x''(n) \rightarrow x''(n-d)$  will be less than  $x''(n-d) \rightarrow x''(n)$ . Thus, the dominant Granger causal influence from  $x''(n-d)$  to  $x''(n)$  would still be inferred from fMRI. Downsampling both  $x''(n)$  and  $x''(n-d)$  by a factor of  $M$ , we obtain  $x''(Mn)$  and  $x''(Mn-Md)$ . It is known that scaling the time index by a factor of  $M$  stretches frequency and contracts time (Crochiere & Rabiner, 1983). Therefore, the delay between the down-sampled fMRI time series  $x''(Mn)$  and  $x''(Mn-Md)$  appears to be less than that between the original LFP time series  $x(n)$  and  $x(n-d)$  with increasing  $M$ , i.e. longer TR. However, it is critical to note that  $d$  was still a factor determining the delay relationship between the fMRI time series. Also, as reported before (Wei, 1982), systematic sampling preserves the direction of causal influence between the variables, though it weakens the magnitude of the relationship between them. The above arguments provide an intuitive explanation for our findings in Fig. 3. Also, preliminary experimental evidence suggests that

latency differences between BOLD data obtained from the right and left visual hemifields reflects the corresponding latency differences in stimulus timing even when the left and right stimuli were barely separated by approximately 100 ms (Katwal, Gatenby, Gore, & Rogers, 2009). Though further experimental research is needed in order to support the preliminary experimental evidence as well as the predictions of our simulations, the discussion presented above provides an intuitive argument in support of our findings.

**With HRF Confound**—Fig. 5 and Fig. 6 illustrate the effect of TR and noise on the detectability of the neuronal delay,  $d_n$ , from GC derived from fMRI as characterized by  $\rho_d$ , in the presence of hemodynamic delays of 0.5 opposing the neuronal delay, for the case of simple delay and simple delay plus intrinsic dynamics, respectively. The corresponding figures for a hemodynamic delay of 2.5 are shown in Fig. 7 and Fig. 8. The negative values of  $d$  indicate that, contrary to the expected dominant Granger causal influence from  $x'(n)$  to  $y'(n)$ , the inferred direction of causality was from  $y'(n)$  to  $x'(n)$ . This corresponds to the situation where in the opposing hemodynamic delay confounded the inference of true causality from fMRI data. In this situation, the point of inflection, defined as the neuronal delay at which mean  $\rho_d$  is greater than 3 and continues to remain so for increasing neuronal delays, is critical and is shown in Table.1.

It is to be noted that the minimum detectable neuronal delays in the presence of opposing HRF confounds given in Table.1 must be only interpreted approximately and no significance should be attached to their exact numerical values. This is because the significance of the causal paths obtained from surrogate data depend on the spectral power in the individual time series, since surrogate data are obtained by retaining the magnitude spectrum of the original time series with only its phase spectrum randomized. The AR model of linearly mixed data is given by a similarity transformation of the original AR matrices and hence is dependent on the spectral power in individual time series (Pandit & Wu, 1983). Consequently, different LFP channels had slightly different points of inflection, as is evident from the standard deviation of the curves in Figs 3–8, since they had different spectral signatures. However, it is to be noted that the range of the standard deviation did not significantly change the point of inflection. Therefore, inferences of significant paths which have large values of  $\rho_d$  will not be affected, though this issue does have a bearing on those values near the threshold (Pandit & Wu, 1983). Consequently, the point of inflection obtained from a different set of experimental data is likely to be numerically different, though its order of magnitude will be similar. In order to shed more practical value to the point of inflection, we have shown in Table.1 how it varies as we raise the threshold from  $\rho_d=2$  (very liberal) to  $\rho_d=4$  (very conservative).

Figs 5 and 7 indicate that for the case of causality induced by a simple delay, neuronal delays which were hundreds of milliseconds were detected even in the worst-case scenario of hemodynamic delays opposing the neuronal delays. Also, comparison of Figs 5 and 6 with Figs 7 and 8 shows that increasing the hemodynamic delay from 0.5 s to 2.5, which are the approximate mean and upper limits of the observed HRF variability reported before (Handwerker, Ollinger, & D'Esposito, 2004), respectively, expectedly raised the point of inflection. However, the dual presence of lower causal influence due to higher proportion of intrinsic dynamics and HRF delay of 2.5 s makes GC applied to fMRI less useful because the corresponding point of inflection was close to or greater than 1 s.

It is counterintuitive that the causal influence inferred from fMRI data for neuronal delays which were hundreds of milliseconds could still be accurate in the presence of opposing hemodynamic delays of up to 2.5 s. Since convolution is a linear time-invariant operation, a temporal shift of the HRF should correspondingly shift the resultant simulated fMRI time series, which would destroy the neuronal causality in fMRI data since the hemodynamic

delays are an order of magnitude greater than neuronal delays. However, our results suggest that the above reasoning is not entirely true. The answer to this apparent contradiction lies in the subtlety of what exactly constitutes a hemodynamic delay. As shown by previous studies (Handwerker, Ollinger, & D'Esposito, 2004), the variability of the HRF across brain regions mainly arises from differences in the shape of the peak, most notably, the time to peak and onset time. As described before, this translates to a variation in the shape parameter of the canonical HRF and we still expect the total duration of the HRF to remain relatively constant. This scenario is not mathematically equivalent to a temporal shift of the HRF and hence the effect of HRF variability on fMRI-based GC analysis was less severe than expected.

**The Effect of Noise**—The results from Figs. 5–8 reinforce the conclusions obtained from Figs. 3–4, that slower sampling and presence of measurement noise reduce the sensitivity of GC obtained from fMRI to shorter neuronal delays. In addition, the differences between the points of inflection obtained with and without noise decreased with increasing TR. This can be explained by the fact that measurement noise is an error between what is measured and what ought to be measured and hence may not be affected to a great extent by the rate of measurement which is represented by the TR. Therefore, the effect of TR was greater on the data in the absence than in the presence of noise. Also, measurement noise is known to introduce spurious causalities (Nalatore, Ding, & Rangarajan, 2007) which may reduce any advantage that might have been gained by sampling faster, as a consequence of which the effect of noise was greater at faster TRs. However, it is noteworthy that more than the point of inflection, noise had a greater effect on the rate of increase of  $\rho_d$  with increasing neuronal delay. It can be seen from Figs 3–8 that once past the point of inflection, the detectability of the neuronal delays improved dramatically with increasing  $d_n$  in the absence of noise as compared to in the presence of noise.

### The Multivariate Case

The network shown in Fig. 2 was correctly inferred from LFP data with 100% accuracy. This is to be expected since the causal structure in the LFP data was artificially introduced. The corresponding fMRI networks with randomized neuronal and hemodynamic delays were detected with accuracies shown in Table.2. As in the bivariate case, the robustness of fMRI-based GC analysis decreased with increasing TR and intrinsic dynamics. It is noteworthy that the accuracy of detecting each of the paths in the multivariate network individually, i.e. the accuracy of detecting a path in the bivariate case, was higher (Table.3) compared to the accuracy of simultaneously detecting all of the paths correctly (Table.2).

The bivariate simulations provided a guideline for choosing scan parameters such as TR given the fact that the neuronal delays and proportion of intrinsic dynamics in the neurophysiological system under investigation and the achievable SNR of the fMRI time series were known *a priori* under the worst-case assumption that the hemodynamic delays opposed the neuronal delays. In contrast, during real experimental situations, researchers typically investigate multivariate brain networks and are constrained by the SNR provided by the scanner, the TR dictated by the requirement of whole brain coverage and the short scanning time available, and the intrinsic dynamics, neuronal and hemodynamic delays inherent in the neurophysiological system under investigation. Therefore, the detection accuracies reported here are critical to determine the confidence that can be placed in multivariate GC networks derived from fMRI, given the SNR, TR and unknown neuronal and hemodynamic delays which are assumed to be in their normal physiological range. Implicit in the randomization of neuronal and hemodynamic delays is the assumption that, contrary to the bivariate case, they may not always oppose one another. Therefore the

multivariate case mimicked the real experimental situations better than the bivariate case, though the latter characterized the constraints and limits of fMRI-based GC analysis.

Although the purpose of the multivariate simulation was to mimic the real situation as closely as possible, the performance of fMRI-based GC analysis in an actual experiment may be better or worse than predicted by us due to the factors outlined below. First, the differences in HRF onset times and time to peak in experimental data may be driven by the underlying neuronal causality and may not always be hemodynamic in nature. Therefore, neuronal causality may explain part of the variance in HRFs across brain regions and hence the situation in experimental data may not be as dire as the one assumed in our simulations where in the hemodynamic and neuronal delays opposed each other in the bivariate case and their variances were mutually exclusive and derived from uniform random distributions in the multivariate case. Second, in experimental data, measurement noise is added only once during the acquisition while in our simulations, it was already present in the LFP data in addition to what we added to the simulated fMRI data. Consequently, the effective SNR of our simulations may be worse than what it seems. Given the above factors, the performance of fMRI-based GC analysis on experimental fMRI data may be better than in our simulations. Contrarily, certain situations may make GC analysis of fMRI perform poorer than in our simulations. For example, pathological conditions may cause extreme discrepancies in HRFs of certain brain regions. David and colleagues (David, et al., 2008) recently reported a situation wherein the hemodynamic response of one of their ROIs in a rat model of absence epilepsy showed an extreme inconsistency by peaking approximately 5 s after the HRFs of other regions and taking more than 30 s as compared to other ROIs to return to baseline. Expectedly, they were not able to infer the correct directionality of the causal influence from raw fMRI data without deconvolving the HRF. Our simulations exclude such situations where in the HRF variability is outside the normal physiological range. If such a situation were to arise, the performance of fMRI-based GC analysis will be worse than that predicted by our simulations. However, in case such a situation is expected in an experimental setting involving a pathological population as in David, et al. (2008), then it is a good idea to obtain simultaneous electrophysiological data to accurately estimate the HRF and deconvolve it before applying Granger causality analysis.

## CONCLUSIONS

In this work, we performed simulations in order to investigate the effects of hemodynamic variability on GC analysis of fMRI data with respect to TR, measurement noise in the data, strength of causal influence and the underlying neuronal delay. We have demonstrated the following: First, in the absence of HRF variability, even tens of milliseconds of neuronal delay can be inferred from GC analysis of fMRI. Second, in the presence of HRF delays which oppose neuronal delays, the minimum detectable neuronal delay may be hundreds of milliseconds. Third, in the more realistic scenario of unknown neuronal and hemodynamic delays within their normal physiological range, the accuracy of detecting the correct multivariate network from fMRI is well above chance and up to 90% with faster sampling. Generically, under all conditions, faster sampling and low measurement noise improved the sensitivity of GC analysis of fMRI data.

## Acknowledgments

The authors acknowledge support by the Georgia Research Alliance and NIH grants R01EB002009 (to XH), R01EY12440 (to KS) and K24EY17332 (to KS).

## References

- Abler B, Roebroeck A, Goebel R, Hose A, Schnfeldt-Lecuona C, Hole G, et al. Investigating directed influences between activated brain areas in a motor-response task using fMRI. *Magnetic Resonance Imaging*. 2006; 24:181–185. [PubMed: 16455407]
- Aguirre G, Zarahn E, D'Esposito M. The variability of human, BOLD hemodynamic responses. *NeuroImage*. 1998; 8:360–369. [PubMed: 9811554]
- Blinowska K, Kus R, Kaminski M. Granger causality and information flow in multivariate processes. *Physical Review E*. 2004; 70:50902–50906.
- Buxton, R. *Introduction to Functional Magnetic Resonance Imaging: Principles and Techniques*. New York: Cambridge University Press; 2002.
- Crochiere, R.; Rabiner, L. *Multirate Digital Signal Processing*. Englewood Cliffs, NJ: Prentice-Hall; 1983.
- David O, Guillemain I, Sallet S, Reyt S, Deransart C, Segebarth C, et al. Identifying Neural Drivers with Functional MRI: An Electrophysiological Validation. *PLoS Biology*. 2008; 6(12):2683–2697. [PubMed: 19108604]
- Deshpande G, Hu X, Stilla R, Sathian K. Effective Connectivity during Haptic Perception: A study using Granger causality analysis of functional magnetic resonance imaging data. *NeuroImage*. 2008; 40(4):1807–1814. [PubMed: 18329290]
- Deshpande G, LaConte S, James G, Peltier S, Hu X. Multivariate Granger causality analysis of brain networks. *Human Brain Mapping*. 2009; 30(4):1361–1373. [PubMed: 18537116]
- Friston K. Functional and effective connectivity in neuroimaging: a synthesis. *Human Brain Mapping*. 1995; 2:56–78.
- Friston K, Harrison L, Penny W. Dynamic causal modeling. *NeuroImage*. 2003; 19(4):1273–1302. [PubMed: 12948688]
- Friston, K.; Holmes, A.; Ashburner, J. *Statistical Parametric Mapping (SPM)*. 1999. [online]: <http://www.fil.ion.ucl.ac.uk/spm/>
- Granger C. Investigating causal relations by econometric models and cross-spectral methods. *Econometrica*. 1969; 37(3):424–438.
- Handwerker D, Ollinger J, D'Esposito M. Variation of BOLD hemodynamic responses across subjects and brain regions and their effects on statistical analyses. *NeuroImage*. 2004; 21:1639–1651. [PubMed: 15050587]
- Kaminski M, Ding M, Truccolo W, Bressler S. Evaluating causal relations in neural systems: Granger causality, directed transfer function and statistical assessment of significance. *Biological Cybernetics*. 2001; 85:145–157. [PubMed: 11508777]
- Katwal, S.; Gatenby, J.; Gore, J.; Rogers, B. Minimum resolvable latency difference of BOLD responses at 7T using autoregressive modeling. *Proceedings of the 17th Annual Meeting of the International Society for Magnetic Resonance in Medicine*; 2009. p. 3677
- Kus R, Kaminski M, Blinowska K. Determination of EEG activity propagation: pair-wise versus multichannel estimate. *IEEE Transactions on Biomedical Engineering*. 2004; 51(9):1501–1510. [PubMed: 15376498]
- Levin J, Frederick B, Ross M, Fox J, von Rosenberg H, Kaufman M, et al. Influence of baseline hematocrit and hemodilution on BOLD fMRI activation. *Magnetic Resonance Imaging*. 2001; 19(8):1055–62. [PubMed: 11711229]
- Levin J, Ross M, Mendelson J, Kaufman M, Lange N, Maas L, et al. Reduction in BOLD fMRI response to primary visual stimulation following alcohol ingestion. *Psychiatry Research*. 1998; 82(3):135–146. [PubMed: 9754438]
- Logothetis N, Pauls J, Augath M, Trinath T, Oeltermann A. Neurophysiological investigation of the basis of the fMRI signal. *Nature*. 2001; 412:150–157. [PubMed: 11449264]
- Nalatore H, Ding M, Rangarajan G. Mitigating the effects of measurement noise on Granger causality. *Physical Review E*. 2007; 75:031123-1–031123-10.
- Noseworthy M, Alfonsi J, Bells S. Attenuation of brain BOLD response following lipid ingestion. *Human Brain Mapping*. 2003; 20(2):116–21. [PubMed: 14505337]

- Pandit, S.; Wu, S. *Time Series and System Analysis with Applications*. New York: John Wiley and Sons; 1983.
- Roebroeck A, Formisano E, Goebel R. Mapping directed influence over the brain using Granger causality and fMRI. *NeuroImage*. 2005; 25:230–242. [PubMed: 15734358]
- Silva A, Koretsky A. Laminar specificity of functional MRI onset times during somatosensory stimulation in rat. *Proceedings of National Academy of Sciences USA*. 2002; 99:15182–15187.
- Stilla R, Deshpande G, Laconte S, Hu X, Sathian K. Posteromedial parietal cortical activity and inputs predict tactile spatial acuity. *Journal of Neuroscience*. 2007; 27(41):11091–11102. [PubMed: 17928451]
- Stilla R, Hanna R, Mariola E, Deshpande G, Hu X, Sathian K. Neural processing underlying tactile microspatial discrimination in the blind: A functional magnetic resonance imaging study. *Journal of Vision*. 2008; 8(10):13.1–19. [PubMed: 19146355]
- Theiler J, Eubank S, Longtin A, Galdrikian B, Farmer D. Testing for nonlinearity in time series: The method of surrogate data. *Physica D*. 1992; 58:77–94.
- Wei W. The effects of systematic sampling and temporal aggregation on causality - A cautionary note. *Journal of the American Statistical Association*. 1982; 77(378):316320.
- Zhuang J, LaConte S, Peltier S, Zhang K, Hu X. Connectivity exploration with structural equation modeling: an fMRI study of bimanual motor coordination. *NeuroImage*. 2005; 25(2):462–470. [PubMed: 15784425]

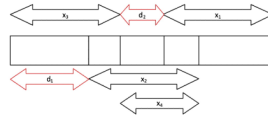


**Figure 1.**

Schematic showing the procedure to derive the four time series of the multivariate network from a single channel of LFP data,  $x(n)$ .  $x_1(n)$ ,  $x_2(n)$ ,  $x_3(n)$  and  $x_4(n)$  represent the four time series derived from  $x(n)$  and  $d_1$  and  $d_2$  represent the inherent neuronal delays in the simulated system governing the relationship between the four time series

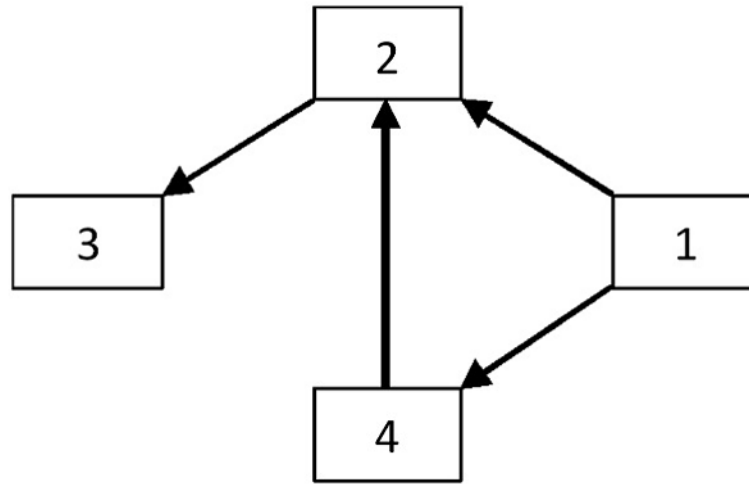


**Figure 2.** The multivariate network expected to be obtained from the time series  $x_1(n)$ ,  $x_2(n)$ ,  $x_3(n)$  and  $x_4(n)$

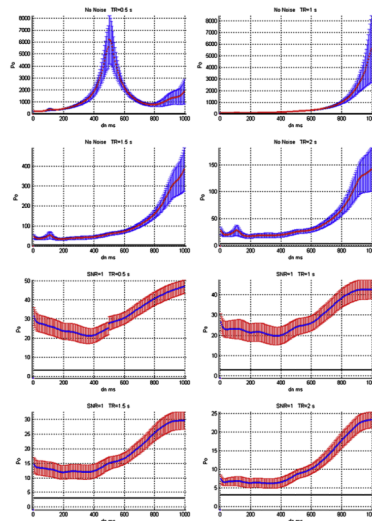


**Figure 3.** Variation of  $\rho_o$ , which determines the detectability of the neuronal influence in the absence of HRF confounds, as a function of neuronal delay  $d_n$ , TR and noise for the case of simple delay. The black line represents the statistical threshold of  $\rho_o=3$

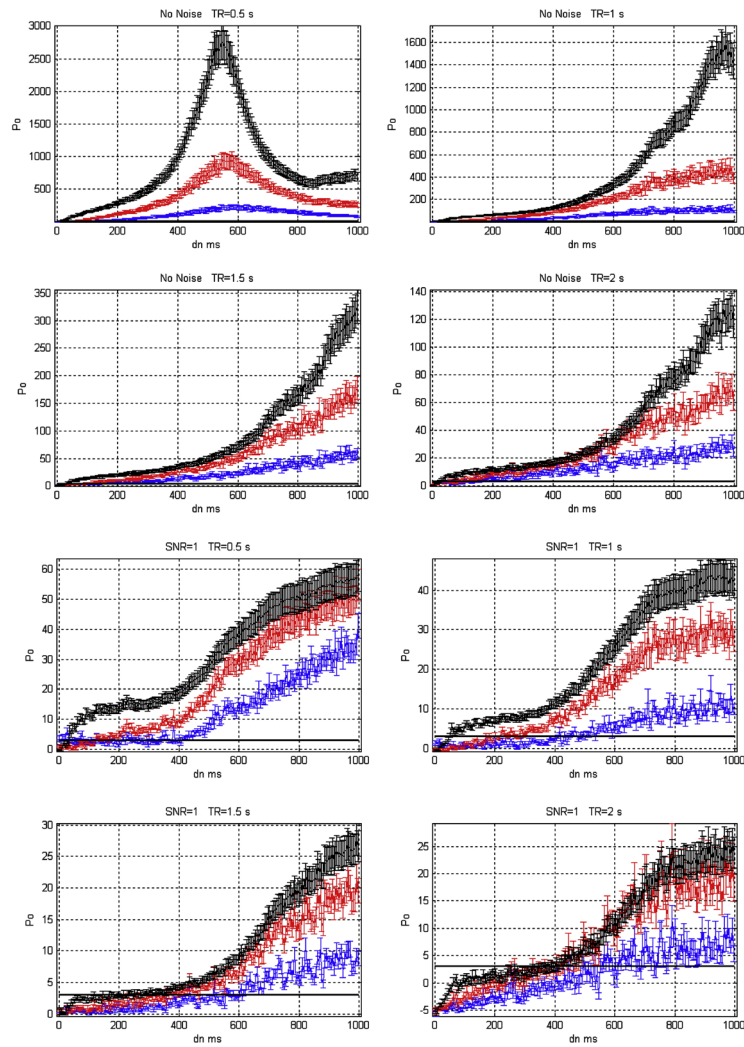


**Figure 4.** Variation of  $\rho_o$ , which determines the detectability of the neuronal influence in the absence of HRF confounds, as a function of neuronal delay  $d_n$ , TR and noise for the case of simple delay plus intrinsic dynamics. The black line represents the statistical threshold of  $\rho_o=3$ . Blue, red and black curves represent  $C$  values of 0.5, 0.7 and 0.9, respectively

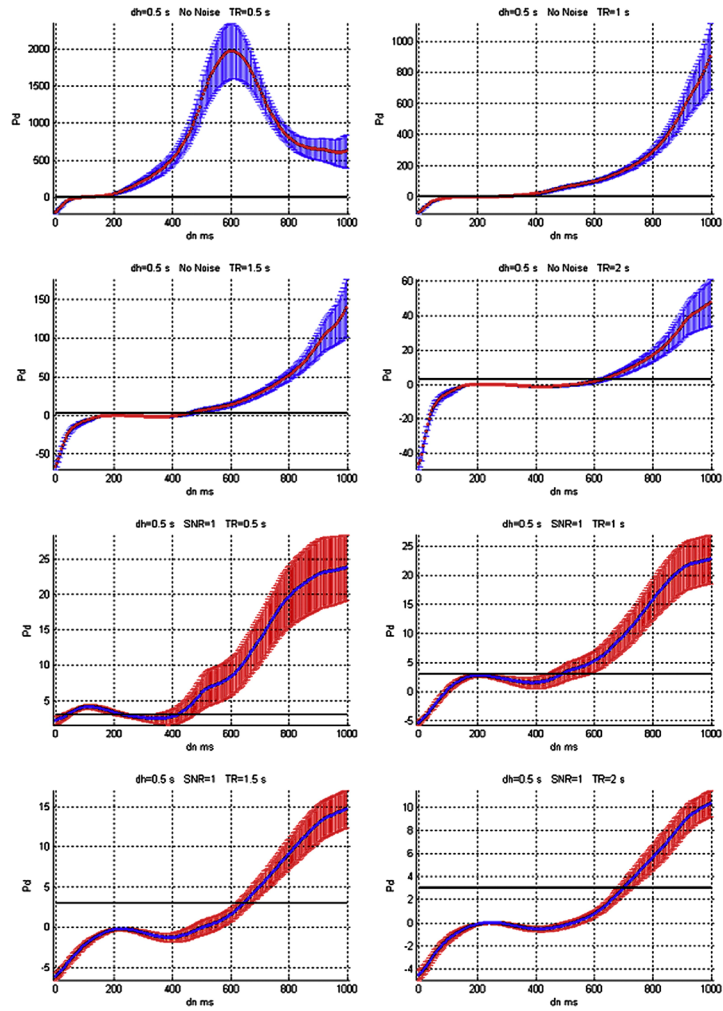


**Figure 5.** Variation of  $\rho_d$ , which determines the detectability of the neuronal influence in the presence of HRF confounds, as a function of neuronal delay  $d_n$ , TR and noise for the case of simple delay. The hemodynamic delay  $d_h=0.5$  s opposed the neuronal delay  $d_n$ . The black line represents the statistical threshold of  $\rho_d=3$

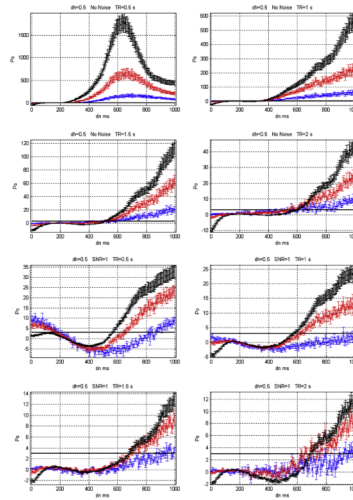


**Figure 6.**

Variation of  $\rho_d$ , which determines the detectability of the neuronal influence in the presence of HRF confounds, as a function of neuronal delay  $d_n$ , TR and noise for the case of simple delay plus intrinsic dynamics. The hemodynamic delay  $d_h=0.5$  s opposed the neuronal delay  $d_n$ . The black line represents the statistical threshold of  $\rho_d=3$ . Blue, red and black curves represent  $C$  values of 0.5, 0.7 and 0.9, respectively.

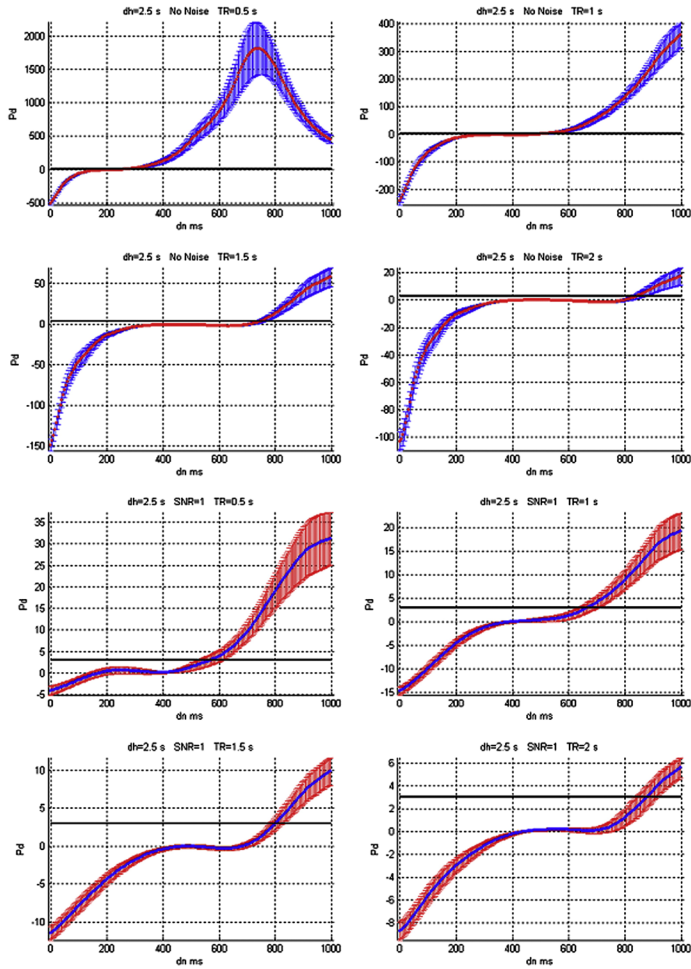


**Figure 7.** Variation of  $\rho_d$ , which determines the detectability of the neuronal influence in the presence of HRF confounds, as a function of neuronal delay  $d_n$ , TR and noise for the case of simple delay. The hemodynamic delay  $d_h=2.5$  s opposed the neuronal delay  $d_n$ . The black line represents the statistical threshold of  $\rho_d=3$

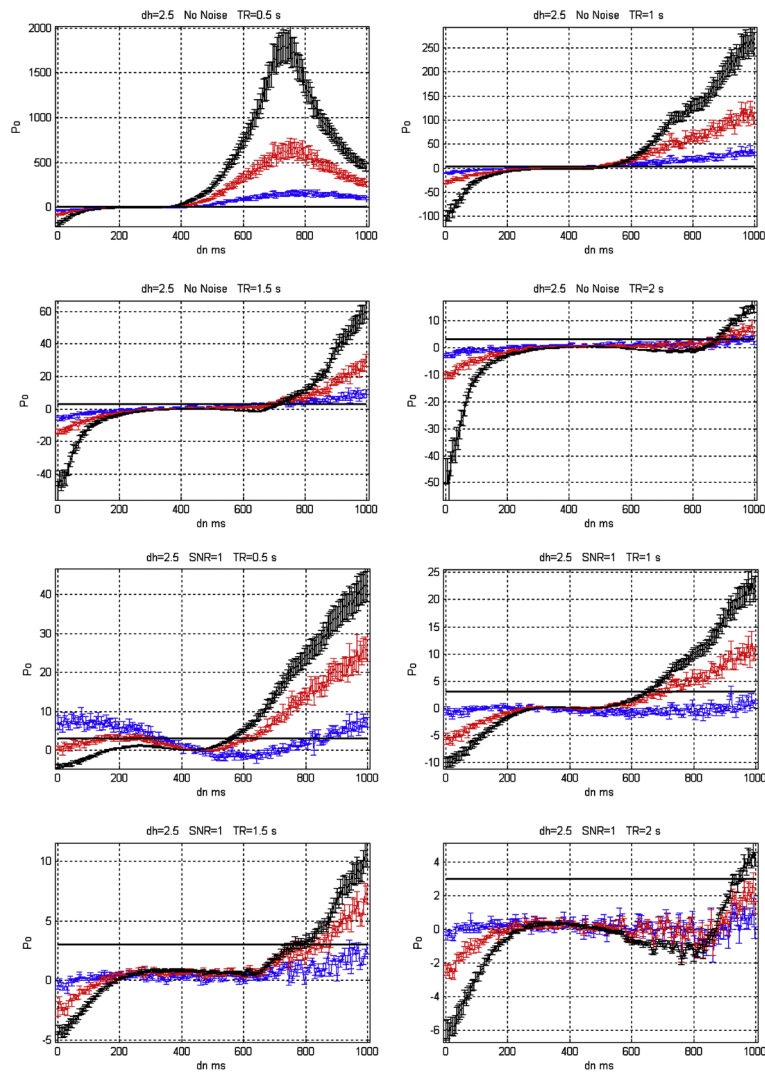


**Figure 8.** Variation of  $\rho_d$ , which determines the detectability of the neuronal influence in the presence of HRF confounds, as a function of neuronal delay  $d_n$ , TR and noise for the case of simple delay plus intrinsic dynamics. The hemodynamic delay  $d_h=2.5$  s opposed the neuronal delay  $d_n$ . The black line represents the statistical threshold of  $\rho_d=3$ . Blue, red and black curves represent  $C$  values of 0.5, 0.7 and 0.9, respectively.

**Table 1**

The points of inflection obtained from the bivariate simulation

TR	$\rho$	Simple Delay						Simple Delay + Intrinsic Dynamics (C=0.9)					
		Without HRF confound		With HRF confound $d_H=0.5$		With HRF confound $d_H=2.5$		Without HRF confound		With HRF confound $d_H=0.5$		With HRF confound $d_H=2.5$	
		No Noise	SNR=2	No Noise	SNR=1	No Noise	SNR=1	No Noise	SNR=1	No Noise	SNR=1	No Noise	SNR=1
0.5	2	5	5	135	405	265	530	10	40	220	560	350	545
	3	5	5	140	420	270	570	10	40	220	570	350	565
	4	5	5	145	455	275	610	15	40	225	580	355	585
	2	5	5	310	450	515	635	15	50	310	555	520	625
1	3	5	5	315	490	525	670	20	55	355	580	530	655
	4	5	5	320	540	535	700	20	75	355	600	535	680
	2	5	5	460	620	740	775	30	150	505	660	710	725
	3	5	5	470	650	750	805	30	285	530	685	725	805
1.5	4	5	5	480	680	760	830	40	385	555	725	730	845
	2	5	5	620	660	830	835	30	325	555	680	875	920
	3	5	5	635	700	845	880	40	405	555	695	885	950
	4	5	5	650	740	860	915	50	435	615	730	890	980
0.5	2	20	120	255	615	375	585	85	415	330	865	420	860
	3	35	175	260	655	380	640	85	415	330	870	435	875
	4	40	205	275	660	380	650	85	455	330	920	435	920
	2	20	200	355	650	480	655	95	450	380	925	490	925
1	3	45	290	365	665	490	715	95	545	380	925	510	990
	4	55	315	365	680	510	775	100	600	400	925	525	>1000
	2	75	365	505	675	685	805	140	560	595	955	765	945
	3	100	435	550	715	755	885	150	620	595	970	805	995
1.5	4	110	490	550	805	765	890	195	690	650	970	890	>1000
	2	85	405	565	680	890	995	110	695	740	920	925	>1000

TR	p	Simple Delay						Simple Delay + Intrinsic Dynamics (C=0.9)					
		Without HRF confound		With HRF confound $d_H=0.5$		With HRF confound $d_H=2.5$		Without HRF confound		With HRF confound $d_H=0.5$		With HRF confound $d_H=2.5$	
		No Noise	SNR=2	No Noise	SNR=1	No Noise	SNR=1	No Noise	SNR=1	No Noise	SNR=1	No Noise	SNR=1
	3	110	475	605	770	920	>1000	165	780	870	995	985	>1000
	4	115	560	620	745	925	>1000	290	785	870	995	995	>1000

**Table 2**

Percentage accuracy of correctly detecting the multivariate Granger causality network from fMRI data

TR	Simple Delay	Simple Delay + Intrinsic Dynamics			Simple Delay + Intrinsic Dynamics Randomized parameter 'C'
		C=0.5	C=0.7	C=0.9	
0.5	90	80	86	87	85
1.0	84	71	74	81	77
1.5	81	69	71	78	72
2.0	72	61	65	68	66

**Table 3**  
 Percentage accuracy of correctly detecting bivariate paths in the Granger causality network obtained from fMRI data

TR	Simple Delay	Simple Delay + Intrinsic Dynamics			Simple Delay + Intrinsic Dynamics Randomized parameter 'C'
		C=0.5	C=0.7	C=0.9	
0.5	92	81	91	94	91
1.0	88	77	75	87	84
1.5	87	69	78	83	76
2.0	86	62	68	82	70